© 2018. Published by The Company of Biologists Ltd | Journal of Experimental Biology (2018) 221, jeb185611. doi:10.1242/jeb.185611

RESEARCH ARTICLE

Synaptic convergence of afferent inputs in primary infrared-sensitive nucleus (LTTD) neurons of rattlesnakes (Crotalinae) as the origin for sensory contrast enhancement

Maximilian S. Bothe[1,2], Harald Luksch[1], Hans Straka[3] and Tobias Kohl[1,*]

ABSTRACT

Pitvipers have a specialized sensory system in the upper jaw to detect infrared (IR) radiation. The bilateral pit organs resemble simple pinhole cameras that map IR objects onto the sensory epithelium as blurred representations of the environment. Trigeminal afferents transmit information about changing temperature patterns as neuronal spike discharge in a topographic manner to the hindbrain nucleus of the lateral descending trigeminal tract (LTTD). A presumed, yet so far unknown neuronal connectivity within this central nucleus exerts a synaptic computation that constrains the relatively large receptive field of primary afferent fibers. Here, we used intracellular recordings of LTTD neurons in isolated rattlesnake brains to decipher the spatio-temporal pattern of excitatory and inhibitory responses following electrical stimulation of single and multiple peripheral pit organ-innervating nerve branches. The responses of individual neurons consisted of complex spike sequences that derived from spatially and temporally specific interactions between excitatory and inhibitory synaptic inputs from the same as well as from adjacent peripheral nerve terminal areas. This pattern complies with a central excitation that is flanked by a delayed lateral inhibition, thereby enhancing the contrast of IR sensory input, functionally reminiscent of the computations for contrast enhancement in the peripheral visual system.

KEY WORDS: Pit organ, EPSP, IPSP, Organotopic organization, Contrast enhancement

INTRODUCTION

Pitvipers (Crotalinae) are able to detect infrared (IR) radiation with loreal pit organs (Noble and Schmidt, 1937). The pits are located bilaterally on the upper jaw between the eyes and the nostrils and allow the detection of electromagnetic waves from 3 to 10 µm (Bullock and Diecke, 1956; Goris and Nomoto, 1967; Moiseenkova et al., 2003). Pitvipers use IR detection in, for example, thermoregulation (Bakken and Krochmal, 2007), predator avoidance (Roelke and Childress, 2007; van Dyke and Grace, 2010) or precise strikes towards warm-blooded prey (Chen et al., 2012; Haverly and Kardong, 1996; Kardong and MacKessy, 1991; Westhoff et al., 2006). Based on the principle of a simple pinhole camera, IR objects are mapped onto the pit membrane (Bakken and Krochmal, 2007; Otto, 1972). This thin sensory layer is innervated by the ophthalmic (N.V1) and the deep (N.V2d) and superficial maxillary (N.V2s) branches of the trigeminal nerve (Bullock and Fox, 1957; Kohl et al., 2014; Lynn, 1931). Each of these pit organ-innervating fiber bundles supplies a distinct sensory region with little overlap of the individual termination areas. Before ramifying within the sensory epithelium, each of the three trigeminal nerve branches split into multiple smaller sub-branches that are interconnected through anastomoses (Kohl et al., 2014). Individual fibers within these sub-branches form brush-like terminal nerve masses (Amemiya et al., 1996; Bullock and Fox, 1957; Goris et al., 1989; Kohl et al., 2014; Terashima et al., 1970) that contain TRPA1 channels for the transduction of IR radiation into electrical signals (Gracheva et al., 2010).

Afferent fibers within N.V1, N.V2s and N.V2d form the major portion of the trigeminal nerve and project into a specific designated area in the most dorsal portion of the rostral hindbrain (Kishida et al., 1982; Kohl et al., 2014). After entering the brainstem in rhombomere 2 (Gilland and Baker, 2005), trigeminal afferent axons from the pit organ form the lateral descending trigeminal tract (lttd) and terminate within the nucleus of the lttd (LTTD; Meszler et al., 1981; Newman et al., 1980; Schroeder and Loop, 1976; Terashima and Liang, 1991). Within this nucleus, afferent terminations form a topographical map that matches the spatial origin of the fibers in the pit membrane (Kohl et al., 2014). Throughout the LTTD, IR afferents form a dense neuropil, within which the somata and dendrites of LTTD neurons are tightly embedded (Kohl et al., 2014; Meszler et al., 1981). Extracellular recordings indicated that the individual receptive fields of the LTTD neurons (Terashima and Goris, 1977) are smaller than those of presynaptic afferent fibers (Desalvo and Hartline, 1978), potentially because of a flanking inhibition (Stanford and Hartline, 1980, 1984). However, the site, neuronal substrate and synaptic mechanism responsible for shaping the dynamics of IR signals in the LTTD are so far unknown.

Here, we studied the synaptic signal processing in LTTD neurons following electrical stimulation of individual trigeminal sub-branches from adjacent areas of the pit membrane. Intracellular recordings of LTTD neurons were made in semi-intact preparations of rattlesnakes with an intact brain and attached pit organs. Electrical stimulation of multiple adjacent small bundles of IR-sensitive afferents at the sensory periphery delineated the spatial representation of sensory signals and the convergence of excitatory and inhibitory IR inputs. The presence of nerve branch-specific response patterns in LTTD neurons suggests that excitatory IR signals in LTTD neurons are contrast enhanced through an asymmetric flanking inhibition in the horizontal plane.

[1]Chair of Zoology, Technical University Munich, Liesel-Beckmann-Str. 4, 85354 Freising-Weihenstephan, Germany. [2]Graduate School of Systemic Neurosciences, Ludwig-Maximilians-University Munich, Großhaderner Str. 2, 82152 Planegg, Germany. [3]Department Biology II, Ludwig-Maximilians-University Munich, Großhaderner Str. 2, 82152 Planegg, Germany.

*Author for correspondence (tobias.kohl@wzw.tum.de)

H.L., 0000-0002-9835-7715; H.S., 0000-0003-2874-0441; T.K., 0000-0002-3757-0555

Received 29 May 2018; Accepted 11 July 2018

Journal of Experimental Biology (2018) 221, jeb185611. doi:10.1242/jeb.185611

MATERIALS AND METHODS

Animals and experimental preparation

In vitro experiments were performed on isolated brain preparations of 22 juvenile western diamondback rattlesnakes (*Crotalus atrox*; Baird and Girard, 1853). Snakes of either sex and a body mass of 23–69 g were obtained from the in-house animal breeding facility at the Chair of Zoology at the Technical University of Munich. Snakes were kept at a temperature of 22–30°C on a 12 h:12 h light: dark cycle. Animals were fed weekly with pre-killed mice and water was provided *ad libitum*. Care and maintenance of the animals followed the established guidelines for venomous snakes (Westhoff, 2014). Electrophysiological experiments were performed *in vitro* on isolated, semi-intact preparations and complied with the 'Principles of animal care', publication no. 86-23, 212 revised 1985 of the National Institutes of Health. Permission for the experiments was granted by the respective governmental institution at the Regierung von Oberbayern (55.2-1-54-2532.6-9-12).

For all experiments, animals were initially anesthetized with isoflurane in an induction chamber. After the tail-pinch reflex ceased, snakes were secured with U-shaped pins to the Sylgard® (Dow Corning, Wiesbaden, Germany) floor of a large Petri dish. Intramuscular injection of a combination of ketamine hydrochloride (40 mg kg^{-1}; ketamine 100 mg ml^{-1}, Ketavet, Zoetis Deutschland GmbH, Berlin, Germany) and xylazine hydrochloride (20 mg kg^{-1}; Rompun 2%, Bayer Vital GmbH, Leverkusen, Germany) ensured deep anesthesia for the subsequent surgical procedure. The body was opened ventrally at the level of the heart and snakes were perfused transcardially with 30–70 ml of ice-cold snake Ringer solution (in mmol l^{-1}: 96.5 NaCl, 31.5 $NaHCO_3$, 4 $CaCl_2$, 2.6 KCl, 2 $MgCl_2$ and 20 D-glucose, pH 7.4). Subsequently, the animals were decapitated and the lower jaws including muscle and connective tissue were removed. The bilateral pit organs in the upper jaw and the innervating trigeminal nerve branches on both sides were maintained intact. Following careful removal of the fangs and associated venomous glands, the skull was opened ventrally to isolate the entire brain with the trigeminal nerve branches and the pit organs on both sides attached (Fig. 1A,B). To mechanically stabilize the trigeminal ganglia, the bone surrounding the latter was kept intact. After completion of the isolation procedure, preparations were stored in ice-cold Ringer solution. For all experiments, the preparations were placed in a recording chamber (2×3 cm) with a volume of ∼6 ml and fixed with insect pins to the Sylgard® floor. Preparations were continuously superfused with oxygenated snake Ringer solution, but with a lower magnesium concentration (in mmol l^{-1}: 0.4 $MgCl_2$) for facilitated activation of NMDA receptors (Nowak et al., 1984). Throughout the experiments, the temperature of the Ringer solution in the chamber was electronically controlled and maintained at 14.0±0.2°C. Whole-brain preparations were used for up to 4 days and kept overnight at 4°C in oxygenated Ringer solution with standard magnesium concentration. No noticeable differences in response parameters were encountered during the daily recording sessions over this period. As a measure for viability of the preparation, we compared the magnitudes of the resting potential following intracellular penetration of neurons recorded on the 3 days after isolation of the brain. There was no significant difference in the mean (±s.e.m.) resting potential over this period (day 1: 61.63±5.10 mV, n=8; day 2: 57.64±4.93 mV, n=6; day 3: 63.10±5.20 mV, n=5; neurons on day 1 versus day 2: P=0.66; neurons on day 2 versus day 3: P=1; neurons on day 1 versus day 3: P=0.75; Mann–Whitney U-test).

Recording of trigeminal nerve afferents and central neurons in the LTTD

At the beginning of each experiment, compound spikes of pit organ-innervating trigeminal afferent fibers as well as presynaptic and postsynaptic field potentials in the LTTD were extracellularly recorded. Glass microelectrodes for these recordings were fabricated with a micropipette puller (P-87 Micropipette Puller, Sutter Instrument, Novato, CA, USA). The electrode tip was broken and the electrodes were then filled with 2 mol l^{-1} sodium chloride to reach a final resistance of 3–5 MΩ. Intracellular recordings from LTTD neurons were performed with glass micropipettes, which after pulling were directly filled with a mixture of 3 mol l^{-1} potassium acetate and 2 mol l^{-1} potassium chloride at a ratio of 9:1, to reach a final resistance of 50–60 MΩ. Electrodes for trigeminal nerve recordings were manually positioned onto a particular nerve branch by 3-axis micromanipulators (U-31 CF, Narishige Group, Tokyo, Japan). For extracellular and intracellular recordings of neuronal activity in the LTTD, electrodes were stereotactically positioned in the horizontal plane and dorso-ventrally advanced stepwise within the brainstem target area with a 3-axis piezo-stepper (Triple Axis Micromanipulator, Sensapex, Oulu, Finland). Neuronal activity of trigeminal nerve fibers and LTTD neurons was recorded (BA-03X, npi electronic GmbH, Tamm, Germany; DAM80, WPI, Sarasota, FL, USA) and digitized (NI USB-6211, National Instruments, Austin, TX, USA) with a sampling rate of 20 kHz using a custom-built Matlab script (Matlab2014a, The MathWorks Inc., Natick, MA, USA). To reduce high-frequency noise, signals were filtered prior to digitizing by low-pass filtering with a cutoff frequency of 13 kHz. Depending on the current intensity, stimulus artifacts were clipped for presentation in the figures.

Electrical stimulation of trigeminal nerve afferent fibers

To access single trigeminal nerve branches, the surrounding connective tissue was removed. For different sets of experiments, either the main branches (N.V1, N.V2d and N.V2s; color coded in Fig. 1B) or up to three adjacent sub-branches of N.V2s were cut with fine scissors and the blunt ends were sucked into glass micropipettes, respectively (Fig. 1C,D). The average distance between the stimulus site of a main nerve branch and the recording site in the central region of the LTTD was 7.7±0.3 mm (n=4). Sub-branches of N.V2s were stimulated more peripherally at an average distance of 12.2±0.8 mm (n=4) between the stimulus site and central LTTD neurons. These values were used to estimate the earliest occurrence of afferent spikes in the brainstem. Micropipettes for suction electrodes were pulled with an electrode puller (P-87 Micropipette Puller, Sutter Instrument) and the tip diameters were individually adjusted to fit the size of each nerve branch by tip cutting and fire polishing. Bipolar single current pulses (0.2 ms, 4–30 µA) were produced by a stimulus isolation unit (Isolated Pulse Stimulator, Model 2100, A-M Systems, Sequim, WA, USA) and applied at a rate of 0.5 Hz. Prior to each recording session, the stimulus threshold (T) of each nerve branch was determined either by recording the spike discharge of the respective nerve branch at a level proximal to the stimulation site (Fig. 1E) or by recording field potentials within the LTTD (Fig. 2).

To differentiate between presynaptic and postsynaptic responses in the LTTD and to calculate the synaptic delay, the conduction velocity of pit organ-innervating afferent fibers was determined. Two glass electrodes were separately placed onto the same nerve branch at defined distances from the stimulus electrode (Fig. 1E). The two electrodes simultaneously recorded evoked compound

Journal of Experimental Biology (2018) 221, jeb185611. doi:10.1242/jeb.185611

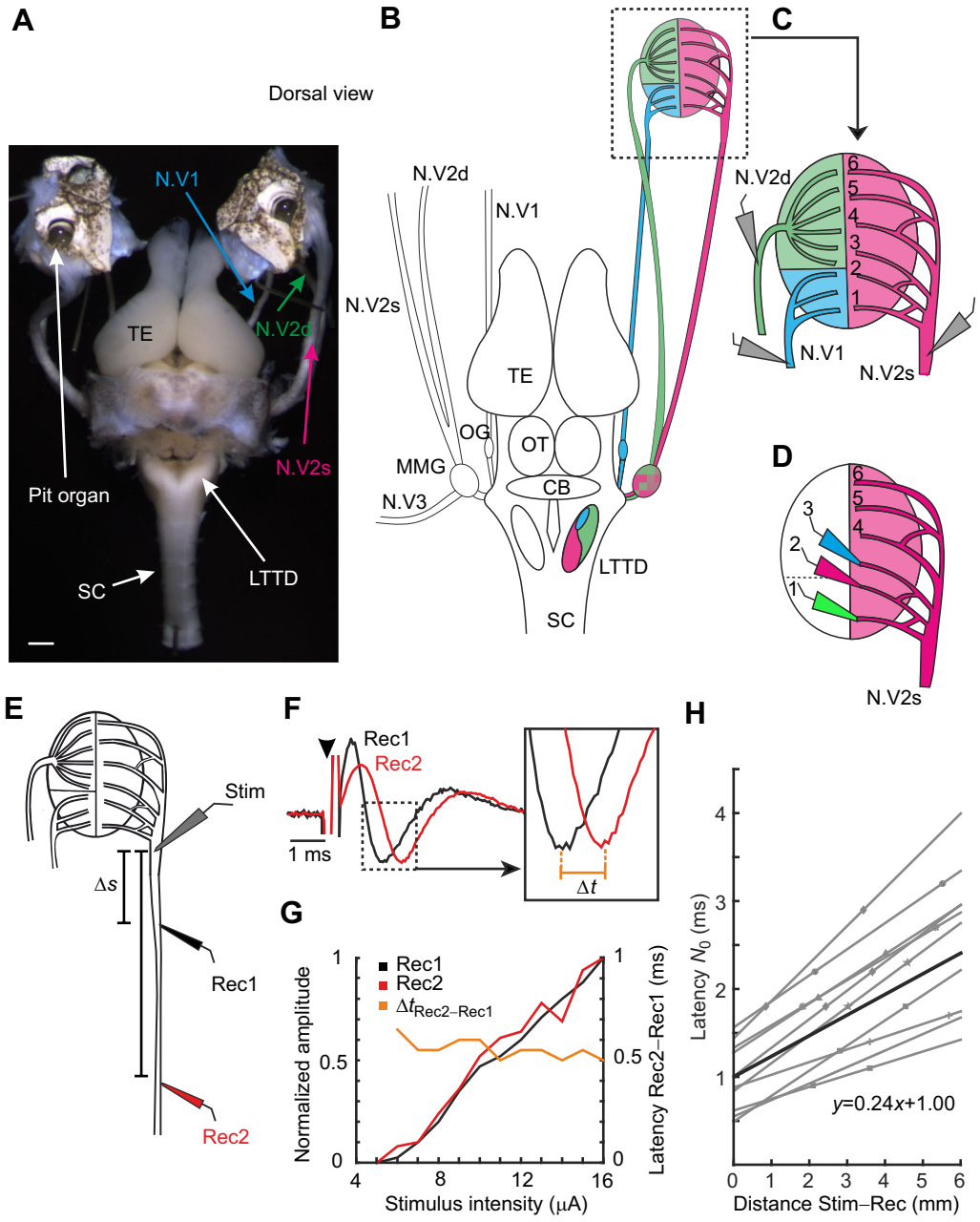

Fig. 1. Isolated rattlesnake whole brain and pit organs for probing infrared (IR) signal processing in the nucleus of the lateral descending trigeminal tract (LTTD). (A) Photograph of an isolated rattlesnake brain with the bilateral pit organs connected via trigeminal nerve branches. TE, telencephalon; SC spinal cord. Scale bar: 1 mm. (B–D) Schematic outline of the brain with color-coded trigeminal nerve innervation of the pit organ (B) by the ophthalmic (N.V1, blue), the deep (N.V2d, green) and superficial maxillary branch (N.V2s, magenta); the topographically organized nerve projection within the LTTD is indicated by corresponding colors. CB, cerebellum; MMG, trigeminal ganglion; OG, ophthalmic ganglion; OT, optic tectum. Higher magnification of the periphery indicates selective stimulation (gray electrodes) of the three main branches (C) or of individual N.V2s sub-branches (color-coded electrodes in D). (E) Schematic diagram depicting the arrangement of stimulus (Stim) and recording electrodes (Rec1, Rec2) for determining conduction velocity and recruitment time of trigeminal afferents. Δs, distance from stimulus electrode to recording electrode. (F) Representative example of compound action potentials in the trigeminal nerve, monitored at Rec1 (black trace) and Rec2 (red trace) after single-pulse stimulation at 3× threshold (T) (arrowhead); the inset depicts the peaks of the two responses and respective delay (Δt) on an expanded time scale. (G) Dependency of normalized compound action potential amplitudes (black and red curves) and time difference (orange curve) of responses at Rec1 and Rec2 (Δt in F) on stimulus intensity of the example shown in F. (H) Dependency of the latency of afferent compound action potentials at Rec1 and Rec2 (n=10) on the respective distance from the stimulus electrode is indicated by individual (gray) and mean (black) linear regression lines of the different pairs; the intersection with the y-axis and the inverse of the slope were used to calculate recruitment time and conduction velocity of trigeminal afferents, respectively. N_0, afferent compound action potential.

action potentials following single-pulse stimulation of the nerve branch at the entrance of the fibers into the pit organ (Fig. 1E). The distance between the two recording electrodes (Fig. 1E) and the difference in the onset of the first negative peak (Fig. 1F, Δt) at the two sites, respectively, were used to calculate the conduction velocity of the fastest trigeminal nerve afferent fibers. While the amplitude increased gradually with increasing current, the time difference between the responses at the two recording sites was

Journal of Experimental Biology (2018) 221, jeb185611. doi:10.1242/jeb.185611

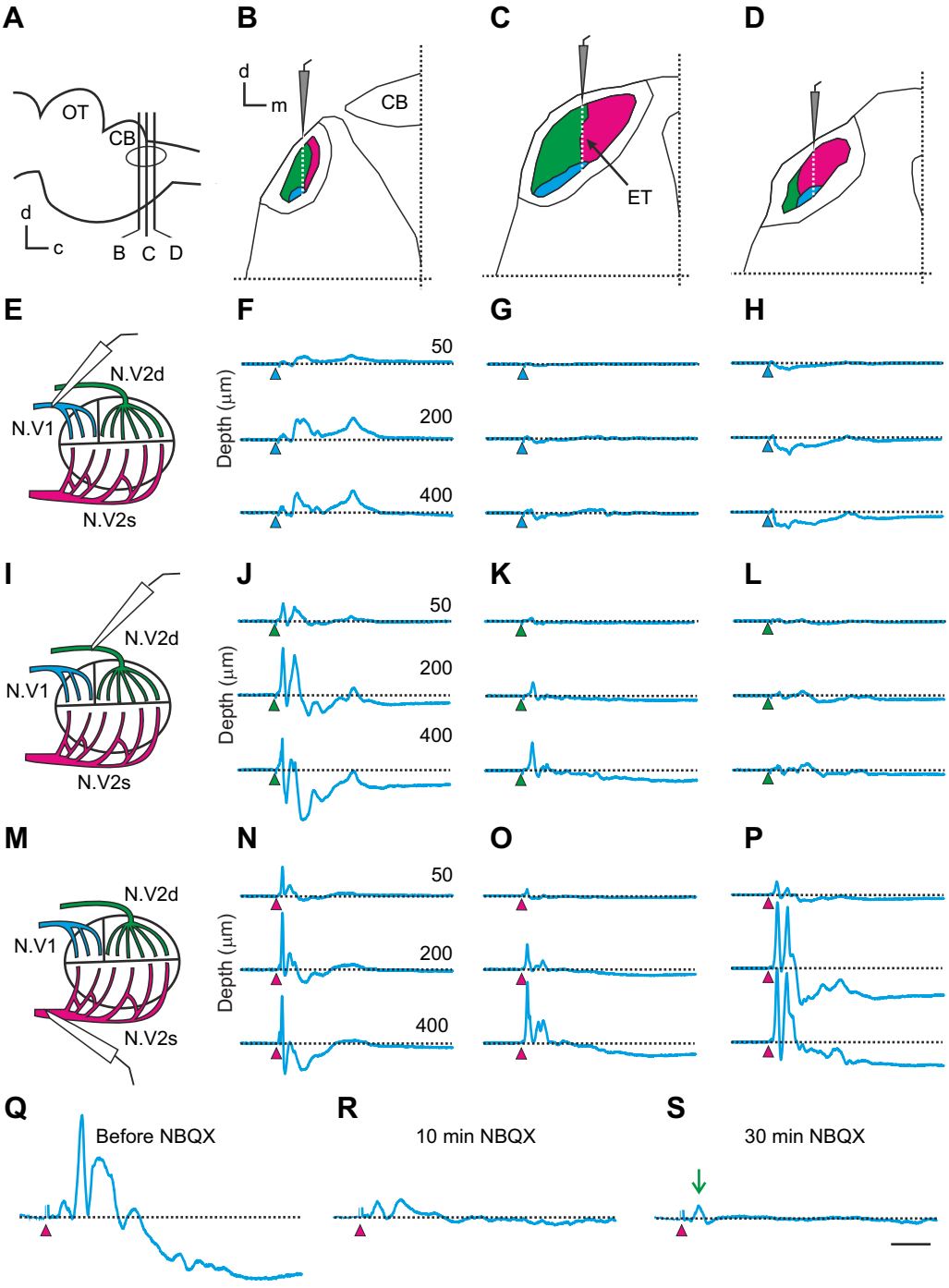

Fig. 2. Topography of trigeminal nerve branch-evoked field potentials in the LTTD. (A–D) Schematic cross-sections of the dorsal hindbrain at three rostro-caudal levels (B–D) illustrating the location of the LTTD (colored area; from Kohl et al., 2014), the segregated termination areas of afferents from N.V1 (blue), N.V2d (green) and N.V2s (magenta) and the electrode tracks (ET) for field potential recordings; the locations of the cross-sections are indicated in the parasagittal section in A. CB, cerebellum; OT, optic tectum; c, caudal; d, dorsal; m, medial. (E–P) Field potentials recorded along dorso-ventral electrode tracks through the rostral (F,J,N), intermediate (G,K,O) and caudal (H,L,P) LTTD, depicted in B–D. Field potentials are exemplarily plotted for a depth of 50, 200 and 400 µm below the dorsal surface, respectively, following electrical stimulation of N.V1 (E–H), N.V2d (I–L) and N.V2s (M–P); colored arrowheads mark stimulus onset. (Q–S) Field potentials in the caudal LTTD at a depth of 200 µm following electrical stimulation of N.V2s, before (Q), and 10 min (R) and 30 min (S) after bath application of the glutamatergic AMPA receptor antagonist NBQX (10 µmol l^{-1}); colored arrowheads mark stimulus onset. Scale bar: 10 ms.

independent of stimulus intensity (orange trace in Fig. 1G). The latency measurements of the compound spikes recorded by the two electrodes also enabled calculation of the recruitment time for the current pulse to trigger action potentials in trigeminal afferents (Fig. 1H).

A putative organotopic arrangement of second-order IR-sensitive neurons within the LTTD was tested by systematically recording field potentials along the rostro-caudal extent of the nucleus following separate stimulation of N.V1, N.V2d and N.V2s (Fig. 1B,C). To distinguish between presynaptic and postsynaptic field potential components, a glutamate blocker of the AMPA receptor subtype, 2,3-dioxo-6-nitro-1,2,3,4-tetrahydrobenzo[*f*]quinoxaline-7-sulfonamide (NBQX disodium salt, 10 µmol l^{-1}; Abcam plc, Cambridge, UK) was bath applied. A complete block of the evoked postsynaptic responses was usually achieved after 25 min. Field potentials were acquired along dorso-ventral depth tracks in steps of 50 µm from the dorsal surface (Fig. 2A–D) at three rostro-caudal positions. These positions were defined relative to the visible swelling of the dorsal hindbrain formed by the LTTD. Accordingly, the central track was located in the center of the swelling while two adjacent tracks were located 150 µm rostral and caudal to this position, respectively.

Statistics

All values are given as means±s.e.m., if not stated otherwise. Statistics and linear curve fitting were performed using a commercial software package (Matlab, R2014b, The MathWorks

Journal of Experimental Biology

Inc.). Statistical differences in parameters were estimated using the Mann–Whitney *U*-test (unpaired parameters).

RESULTS

Temporal parameters of evoked trigeminal nerve activity

Electrical single-pulse stimulation of N.V2s or N.V2d (n=10) close to the pit organ elicited compound action potentials in the respective nerve branches with a characteristic waveform (Fig. 1E,F). Simultaneous recordings of the same nerve branch at two different positions relative to the stimulus electrode (Rec1 and Rec2 in Fig. 1E) allowed determination of basic parameters for electrical activation of spikes in trigeminal afferents. Plotting the amplitude of the evoked negativity peak as a function of stimulus intensity (see representative example in Fig. 1F) yielded the average current threshold for activating IR-sensitive trigeminal afferents (4.1±0.8 µA; n=10). The linear growth of the peak response amplitude with increasing current intensity (black and red curve in Fig. 1G) complies with a gradual recruitment of larger numbers of fibers once the activation threshold of the most susceptible fibers has been reached. Moreover, dual recordings of evoked compound spike activity of trigeminal nerve afferents at two distances from the stimulus site (Rec1 and Rec2 in Fig. 1E) allowed estimation of the conduction velocity of these fibers and the recruitment time for electrical activation. Independent of stimulus magnitude, the delay Δt between the peak negativities, measured simultaneously at the two recording sites (black and red trace in Fig. 1F), was largely intensity invariant and amounted in the typical example to 0.5–0.6 ms (orange trace in Fig. 1G). Plotting the latency of the two negativity peaks as a function of the distance Δs between stimulus and recording electrodes (Fig. 1H) yielded an average recruitment time for trigeminal afferents of 1.0±0.1 ms and a conduction velocity (inverse slope) of 4.2±0.6 m s^{-1} (n=10) at the recording temperature of 14.0±0.2°C.

Field potential recordings in the LTTD

Systematic recordings of field potentials at three levels along the rostro-caudal extent of the LTTD in the dorsal hindbrain (Fig. 2A–D) following separate electrical stimulation of N.V1, N.V2d and N.V2s (Fig. 2E,I,M) revealed a differential trigeminal nerve branch-specific regional distribution of the amplitudes. The different depth profiles of the field potentials evoked by the three nerve branches, shown in a representative example in Fig. 2, suggests the presence of a rostro-caudal and dorso-ventral topography of nerve branch-specific synaptic inputs to LTTD neurons. The rostral part of the LTTD (Fig. 2B) was dominated by synaptic activity from N.V2d (Fig. 2J), even though an activation of N.V1 and N.V2s also caused noticeable field potentials in this area, although with different waveforms (Fig. 2F,N). Neurons in the central part of the LTTD (Fig. 2C) predominantly received inputs from N.V2s (Fig. 2O), with minor contributions from N.V1 and N.V2d (Fig. 2G,K). The caudal part of the LTTD (Fig. 2D) was dominated by inputs from N.V2s (Fig. 2P) even though stimulation of N.V1 also evoked field potentials in this area, but with smaller amplitudes (Fig. 2H). Independent of the rostro-caudal position of the recording electrodes, field potentials were generally larger in central and ventral areas of the LTTD (e.g. Fig. 2J,P) with an additional nerve branch-specific activation of longer-latency components, indicating a nerve branch- and/or region-specific activation of polysynaptic responses. Bath application of NBQX, a glutamatergic AMPA receptor antagonist (Fig. 2Q–S) blocked all responses, except for a small initial component (green arrow in Fig. 2S) that probably reflects presynaptic spiking of afferent fibers with an onset of ∼3 ms (2.9±0.1 ms, n=5). This latency is compatible with the delay expected from the known afferent conduction velocity, stimulus recruitment time and distance between stimulus and recording site (see above for values). The complete block of all postsynaptic responses suggests that trigeminal afferent-evoked glutamatergic activation of LTTD neurons is largely mediated by AMPA receptors.

The obvious predominance of N.V2s-evoked field potentials across the LTTD corresponds to the larger size of the innervated peripheral area by this nerve branch, which extends throughout half of the sensory epithelium of the pit organ (see nerve branches in magenta in Figs 1B, 2M). In addition, the differential distribution of field potentials within the LTTD, activated from the three nerve branches, complies with their respective anatomical termination pattern within this hindbrain area (Kohl et al., 2014). The matching morpho-physiological distribution of IR signal representations within the LTTD therefore complies with a central sensory topography of afferent synaptic inputs, which in the subsequent sets of experiments was used to guide the location of intracellular recordings.

Excitatory and inhibitory synaptic responses in LTTD neurons

The response profile of LTTD neurons was determined by intracellular and juxtacellular recordings following electrical single-pulse stimulation of up to three individual, anatomically adjacent N.V2s sub-branches (Fig. 1D). This allowed probing of the convergence of synaptic inputs in LTTD neurons from neighboring peripheral origins (Fig. 1D). The resting membrane potential of the recorded neurons (n=21) spanned a wide range (between −39 and −83 mV), with the lowest values for juxtacellular recordings. Generally, cells with a low resting membrane potential were stabilized after penetration by hyperpolarization to about −55 mV. The dynamics of the responses was characterized by activating synaptic potentials from each N.V2s sub-branch with gradually increasing current pulse intensity. At very low stimulus intensities, immediately above threshold (∼4.5 µA), the responses in most cells consisted of short-latency EPSPs with synchronized onsets during successive stimulus trails (Fig. 3Ai and inset). With increasing strength of the current pulses, these EPSPs triggered single (Fig. 3Aii) or multiple action potentials with delays of up to ∼30 ms for action potentials with the longest latency (Fig. 3Aiii,B), indicative of polysynaptic excitatory components. The delay of the first spike consistently matched that of the EPSPs and was similarly independent of the peripheral origin from a particular N.V2s sub-branch. The latency of the excitatory inputs from the three sub-branches in a given neuron ranged from 5.4 to 7.6 ms (6.4±0.1 ms; n=32). In order to determine the number of intercalated synapses between the electrically stimulated afferent fiber bundle and the recorded LTTD neuron, we first estimated the latency of presynaptic trigeminal afferent responses in the LTTD based on the known recruitment time, conduction velocity and distance between stimulus and recording site (see above for values). The difference (∼1 ms) between the calculated delay of 3.9 ms and the actual presynaptic field potential component of 2.9 ms is due to the more distal stimulation of N.V2s sub-branches (∼4 mm) in the case of intracellular recordings. Assuming a delay of 1.8–2.0 ms for the synaptic transmission as previously reported in isolated amphibian brain preparations at the same temperature, i.e. 14°C (Straka et al., 1997), the theoretically calculated latency of 5.9 ms for trigeminal nerve-evoked synaptic responses in LTTD neurons thus corresponds to the actual onset of the measured short-latency EPSPs and spikes, confirming a monosynaptic origin.

Journal of Experimental Biology (2018) 221, jeb185611. doi:10.1242/jeb.185611

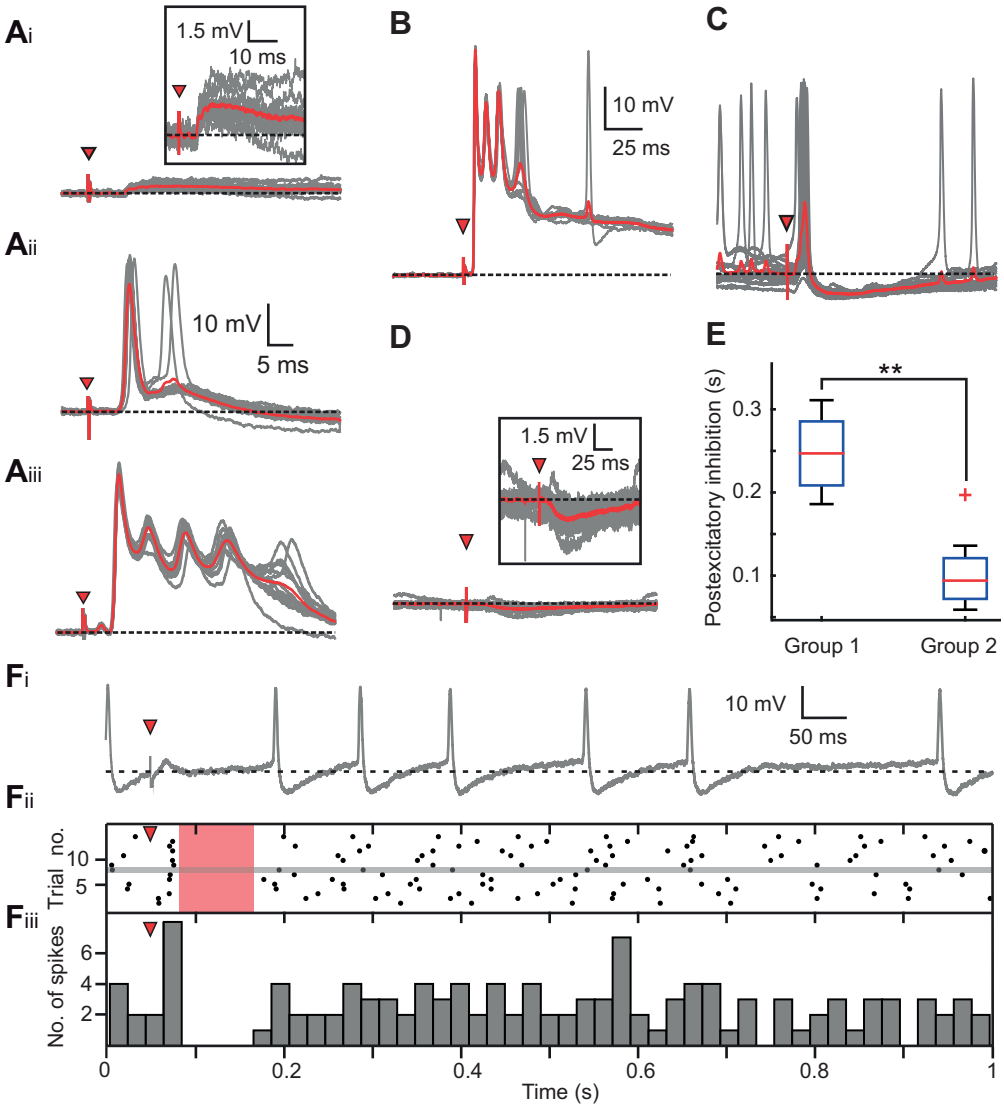

Fig. 3. Spectrum of trigeminal afferent-evoked synaptic responses in LTTD neurons. (A) Superimposed single sweeps (gray) and averages of synaptic responses (15 trials each, red) in a LTTD neuron following current pulse stimulation of N.V2s$_1$; with increasing stimulus intensity, responses changed from short-latency excitatory postsynaptic potentials (EPSPs; Ai, 1.05×*T*) to single (Aii, 1.1×*T*) and multiple action potentials (Aiii, 1.4×*T*). (B–D) Single sweeps (gray) and averages of synaptic responses (15 trials each, red) recorded from three LTTD neurons following current pulse stimulation (3×*T*) of N.V2s$_1$ (B), N.V2s$_2$ (C) and N.V2s$_3$ sub-branches (D); synaptic responses consisted of a short-latency, sustained excitation with multiple spikes (B), short-latency single spikes followed by inhibitory components (C) or longer-latency inhibitory postsynaptic potentials (IPSPs) without a preceding excitatory component (D); boxed insets in Ai and D show EPSPs and IPSPs on expanded amplitude and time scales, respectively. (E) Extent of post-stimulus silencing of spontaneous activity following current pulse stimulation of individual N.V2s sub-branches that caused multiple (group 1, *n*=4) or single short-latency spike activity (group 2, *n*=15); ***P*<0.01, Mann–Whitney *U*-test. (F) Single sweep of a synaptic response in a LTTD neuron (Fi) evoked by electrical pulse stimulation of N.V2s$_4$; the spike event plot for successive trials (*n*=15; Fii) and corresponding post-spike histogram (bin width: 20 ms; Fiii) illustrate a robust inhibitory period (light red area) following the initial synchronized spike discharge. Red triangles in A–D,F indicate electrical pulses. Calibration bars in Aii also apply to Ai and Aiii; calibration bars in B also apply to C,D.

In a smaller number of neurons, electrical pulse stimulation of N.V2s sub-branches evoked either a single, monosynaptic spike followed by a prolonged hyperpolarization of varying magnitude and duration (Fig. 3C) or a distinct longer-latency IPSP without preceding monosynaptic excitation (*n*=8; Fig. 3D and inset). The delayed IPSPs had an average latency of 15.1±0.5 ms (*n*=8) and therefore were at least of disynaptic origin. However, independent of the presence or absence of a preceding monosynaptic excitation, inhibitory postsynaptic components only became visible at the highest employed stimulus intensity (3×*T*, i.e. 3 times the current stimulus threshold intensity to evoke nerve potentials; see above for values), compatible with an intercalation of at least two synapses between the stimulation site and the recorded LTTD neuron. Spontaneously active neurons (*n*=7) allowed estimation of the temporal extent of the delayed inhibition on the firing rate (Fig. 3F). While all such neurons exhibited a stimulus-driven silencing of the resting discharge, the duration of the latter post-stimulus inhibition varied from 60 to 310 ms (137±20 ms; red area in Fig. 3Fii), depending on the stimulated N.V2s sub-branch (*n*=15). Nerve branches that evoked a pronounced preceding monosynaptic excitation with multiple spikes upon electrical pulse stimulation (e.g. Fig. 3Aiii,B) also caused significantly longer periods of post-excitatory inhibition in the recorded neurons (group 1, *n*=4 in Fig. 3E) compared with nerve branches, which activated only single spikes or exclusively inhibitory responses (e.g. Fig. 3C,D; group 2, *n*=11 in Fig. 3E; Mann–Whitney *U*-test, *P*=0.0029). This effect is

Journal of Experimental Biology (2018) 221, jeb185611. doi:10.1242/jeb.185611

probably related to the fact that a more effective monosynaptic activation also more effectively recruited local interneurons through which a feed-forward inhibition is potentially mediated (e.g. Biesdorf et al., 2008). However, independent of the dynamics, the presence of a prolonged period of post-stimulus inhibition of spike activity as illustrated in the representative example in Fig. 3Fiii was common to all recorded LTTD neurons.

Convergence pattern of synaptic inputs from multiple N.V2s sub-branches

The recording of synaptic responses following separate electrical pulse stimulation of two or three peripheral sub-branches of N.V2s (i.e. N.V2s$_{1–3}$, N.V2s$_{2–4}$ or N.V2s$_{4,5}$; see color-coded stimulus electrodes in Fig. 1D) allowed characterization of the convergence of signals from spatially adjacent areas of the pit membrane in individual LTTD neurons (n=19). The predominating response in almost all neurons was a monosynaptic excitation from at least one sub-branch that triggered single or multiple action potentials. The majority of these neurons (n=13) also exhibited additional synaptic responses from adjacent sub-branches that, however, differed in their dynamics as illustrated by the three typical examples shown in Fig. 4A–C. Only a few LTTD neurons (n=6) were encountered in which each of the adjacent sub-branches evoked an excitation with similar spike discharge dynamics. The synaptic responses, separately evoked from adjacent sub-branches, e.g. N.V2s$_{1–3}$ (Fig. 4A–C) usually consisted of a long-latency inhibition with or without preceding monosynaptic excitation (Fig. 4Ai) and excitatory responses from the two other sub-branches (Fig. 4Aii,iii). However, the relative synaptic weight of excitatory and inhibitory components differed between inputs from different sub-branches as well as between different neurons (see responses in Fig. 4Bi–iii,Ci–iii). Even though the contributions of excitatory and inhibitory responses varied with respect to amplitude and duration, most recorded neurons received a dominant excitation from at least one of the two or three tested N.V2s sub-branches (Fig. 4Aiii,Bii,Ci).

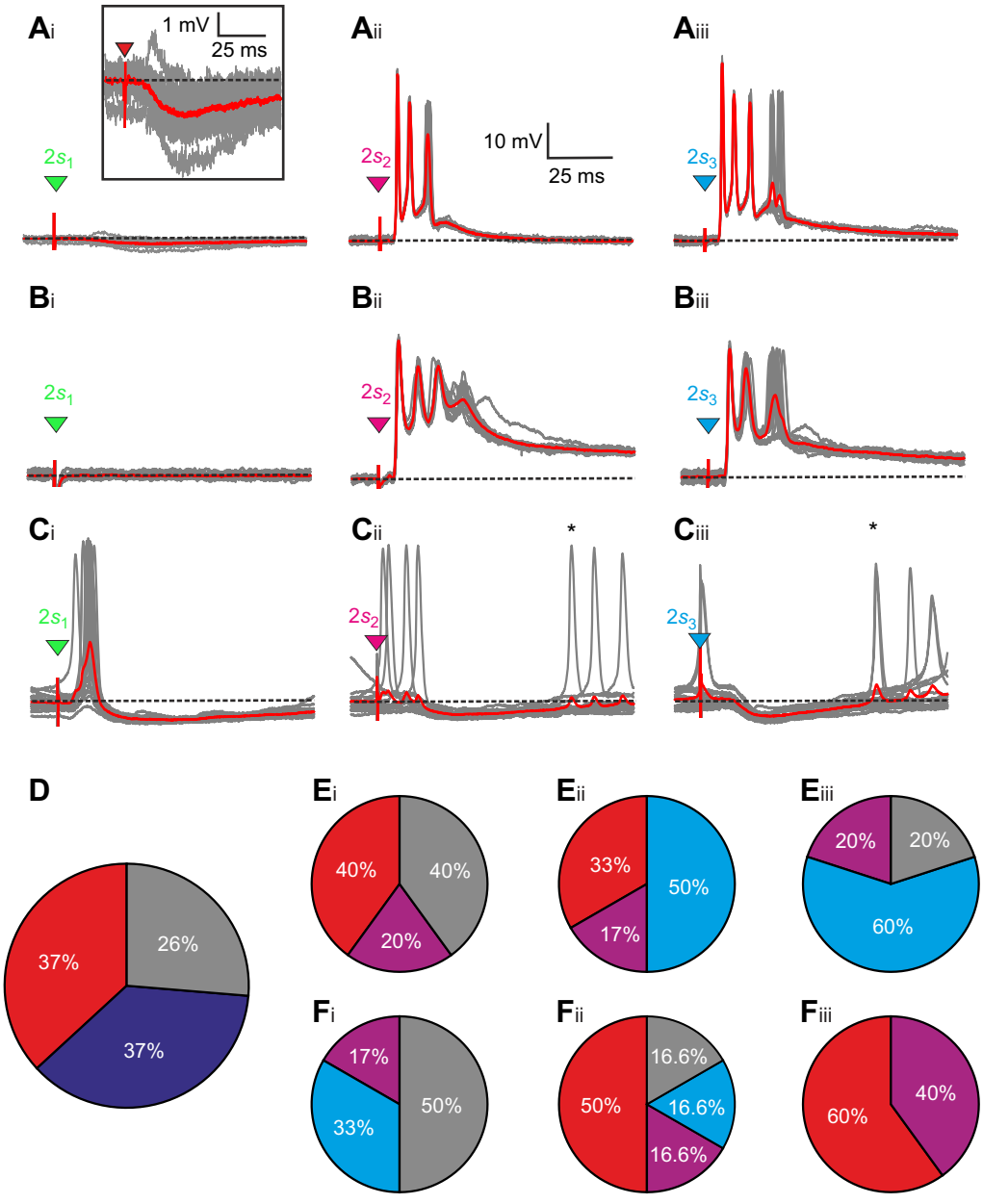

Fig. 4. Convergence pattern of synaptic responses from adjacent N.V2s sub-branches in LTTD neurons. (A–C) Superimposed single sweeps (gray) and averages of synaptic responses from the three sub-branches (15 successive trials each, red) in each of the three LTTD neurons (Ai–Aiii, Bi–Biii, Ci–Ciii); note the different convergence pattern of the three inputs in each neuron; boxed inset in Ai shows synaptic responses on an expanded amplitude and time scale. Green, red and blue triangles in A–C indicate electrical pulses applied to the respective color-coded N.V2s$_{1–3}$ as shown in Fig. 1D. (D) Distribution of neurons (n=19) classified by a temporal or nasal pit membrane origin of convergent sub-branch-specific excitatory and inhibitory inputs. In 37% of neurons, the excitation originated from more rostral sub-branches (dark blue sector) and the inhibition from more caudal sub-branches; in another 37% of neurons (red sector), this pattern was inverted; and in 26% of neurons (gray sector), no trend was visible. (E,F) Distribution of strong excitation (red sectors), weak excitation (purple sectors) and inhibition (light blue sectors) among inputs from temporal (Ei, Fi), intermediate (Eii, Fii) and nasal regions of the pit membrane (Eiii, Fiii); the distribution is separately plotted for neurons with a dominating excitation from temporal (Ei–Eiii) or nasal regions of the pit membrane (Fi–Fiii); gray sectors indicate the absence of a response.

Journal of Experimental Biology (2018) 221, jeb185611. doi:10.1242/jeb.185611

Excitatory and inhibitory inputs in different LTTD neurons could originate from any one of the electrically stimulated sub-branches. Accordingly, the recorded LTTD neurons were differentiated into three groups. In neurons of the first group (~37%; red sector in Fig. 4D), excitatory inputs derived from a more caudal and inhibitory inputs from a more rostral area of the pit membrane. In these neurons, the synaptic inputs from interjacent sub-branches gradually shifted from a dominating excitation (red sectors in Fig. 4Ei–iii) to a dominating inhibition (light blue sector in Fig. 4Ei–iii). In a similarly large group of neurons (~37%), this pattern was inverted and consisted of an excitation that originated from more rostral sub-branches (dark blue sector in Fig. 4D) with a corresponding transition to a more caudal origin of inhibitory inputs (see red and light blue sectors in Fig. 4Fi–iii). In the remaining ~26% of neurons, the excitation had no predominant rostro-caudal origin (gray sector in Fig. 4D). The sub-branch-dependent transition from excitatory to inhibitory inputs in the first two groups of neurons appeared to be accompanied by an alteration in the extent of the delayed inhibition. The validity of this impression was confirmed in spontaneously active neurons, where the duration of the silent period was determined as the interval between the stimulus and the onset of the first spike after the post-excitatory period (asterisk in Fig. 4Cii,iii). Dominant inhibitory inputs persisted on average for ~150 ms (151±33 ms; n=8), while weaker inhibitory responses from adjacent sub-branches lasted only ~110 ms (112 ±28 ms; n=8).

DISCUSSION

Afferent and synaptic signals from the pit organ are topographically represented within the first central nucleus in the rattlesnake hindbrain. Synaptic responses in LTTD neurons following electrical stimulation of multiple peripheral axonal fiber bundles consist of short-latency excitatory and delayed inhibitory responses. The relative magnitudes of the two components systematically differ for adjacent trigeminal sub-branches. The convergence of excitatory and adjacent inhibitory inputs in single LTTD neurons complies with a central activation flanked by a lateral inhibition. This is compatible with a contrast enhancement of IR objects and the origin of the receptive field size reduction previously observed in LTTD neurons (Stanford and Hartline, 1984). The topography of excitatory and inhibitory inputs suggests a representation of sensory signals in individual LTTD neurons that depends on an enhancement of peripheral synaptic inputs from horizontally adjacent areas of the pit membrane, functionally similar to center-surround interactions in the peripheral visual system (Cook and McReynolds, 1998; Enroth-Cugell and Lennie, 1975). Moreover, the sub-branch-specific ratio between excitatory and inhibitory response components revealed an asymmetric magnitude of the delayed inhibition upon stimulation of adjacent sensory areas. Such an asymmetric influence of inhibitory response components from neighboring sensory compartments has previously been described as the origin of directional motion encoding in retinal circuits (Barlow and Levick, 1965; Briggman et al., 2011) and might therefore represent the first step in the processing of moving IR stimuli in the rattlesnake hindbrain.

Synaptic processing of IR signals in LTTD neurons

A major organizational principle of IR object processing in the rattlesnake hindbrain is the topographical representation of sensory signals from the pit organ epithelium along the rostro-caudal and medio-lateral extent of the LTTD (Fig. 2). The distinct spatial pattern of electrically activated synaptic responses within the morphological limits of the LTTD complies with the region-specific termination of pit organ-innervating trigeminal afferents (Kohl et al., 2014). Accordingly, IR signals form a sensory map along the rostro-caudal extent of the hindbrain comparable to, for example, visual signals within the optic tectum (Dräger and Hubel, 1976; Heric and Kruger, 1965; Stanford and Hartline, 1984) rather than a motor map such as for vestibular signals in the adjacent hindbrain area (Chagnaud et al., 2017). Major hallmark features of the region-specific central IR object representation are complex, yet dynamically structured synaptic responses that derive from predictable combinations of EPSPs and IPSPs in compliance with results from previous extracellular recordings (Stanford and Hartline, 1984). The complexity of the synaptic responses suggests that stimulation of regionally restricted epithelial areas in the horizontal plane activates microcircuit modules that cause the monosynaptic afferent excitation of LTTD neurons to be dynamically shaped and temporally modified by a superimposed longer-latency inhibition that derives from adjacent pit membrane regions (Fig. 5).

The truncation of the excitation in central LTTD neurons by a delayed inhibition (Fig. 5C) reinforces transient central excitatory representations of IR signals, similar to the dynamic enhancement of phasic vestibular signals by local inhibitory circuits (Biesdorf et al., 2008). Common to both sensory systems is the mediation of the delayed inhibition by a disynaptic side-loop, presumably through local populations of GABA and/or glycinergic

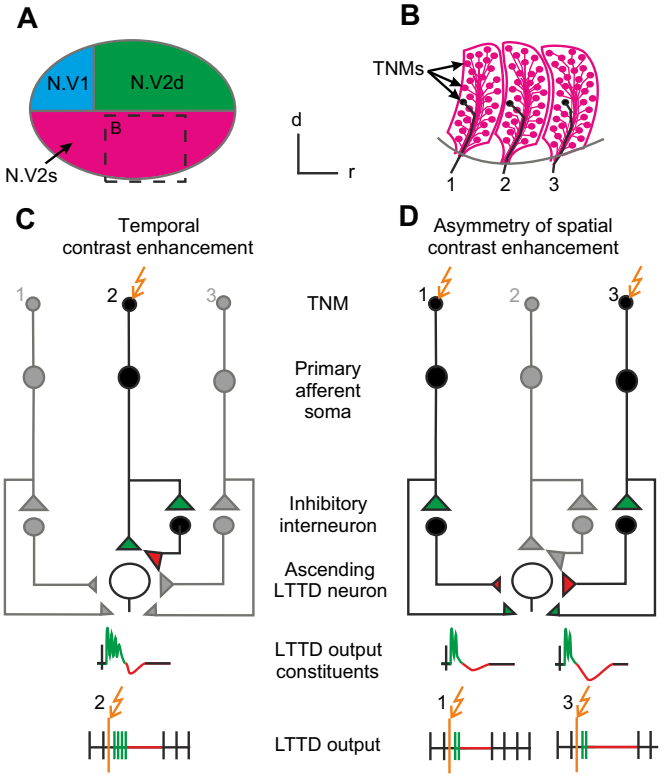

Fig. 5. Putative organization of the LTTD microcircuitry. (A,B) Schematic diagram of the pit membrane (A) and structure of the area (B) supplied by three N.V2s sub-branches (magenta); one terminal nerve mass (black) of each sub-branch defines the receptive area (1–3 in B). d, dorsal; r, rostral. (C) Schematic circuit diagram and synaptic responses illustrating the convergence of monosynaptic EPSPs/spikes and disynaptic IPSPs in LTTD neurons for temporal sharpening of IR signals. (D) Schematic circuit diagram and synaptic responses summarizing the asymmetric convergence of EPSPs/spikes and IPSPs from spatially adjacent receptive areas as a potential substrate for IR contrast enhancement, edge detection and motion encoding. TNM, terminal nerve mass.

interneurons. This inhibition therefore contributes to a short-term silencing during ongoing IR motion stimulation of the sensory periphery that accompanies a long-term adaption that has been demonstrated to occur in primary afferents over a period that ranges up to 30 s (Bullock and Diecke, 1956; de Cock Buning et al., 1981). The activation of variable sequences of excitatory and inhibitory synaptic response components in the present intracellular recordings not only complies with but also further extends previous findings obtained by extracellular recordings (Stanford and Hartline, 1984). The intracellular recordings in this study in fact demonstrate a sequential activation as well as a spatial convergence of excitatory and inhibitory response components in neurons of the LTTD circuitry by single-pulse stimulation of individual pit membrane-innervating trigeminal nerve branches (Fig. 5C,D). This computation is in accordance with the idea that the receptive field of LTTD neurons is shaped by an excitation that is spatially (Fig. 5C) as well as temporally flanked by an inhibition (Fig. 5D). The spatially specific inhibition from adjacent peripheral sensory areas (Fig. 5D) is well suited for contrast enhancement of IR object representations, while the temporally delayed inhibition complies with an early stage of IR edge detection and motion recognition.

IR contrast enhancement in LTTD neurons

Independent of the pit organ optics, trigeminal IR-sensitive afferent fibers transmit heat flux-related signals, which reflect the temperature contrast between the background and emerging objects with a different radiation signature (Bullock and Diecke, 1956; Goris and Nomoto, 1967; Terashima et al., 1968). This is comparable to the spike discharge pattern of retinal ganglion cells, which also reflects stimulus contrast-related interactions between ON and OFF bipolar cell responses (Kuffler, 1953; Rodieck, 1965). The encoding of IR contrast differences at the first, afferent fiber level is obviously further enhanced in LTTD neurons by local inhibitory circuitries that functionally generate the equivalent of a center-surround interaction in the horizontal plane (Fig. 5D). These putative networks assist in the spatio-temporal integration of excitatory and inhibitory response components, thereby increasing the neuronal signals that encode the contrast between an emerging stimulus and the background at the single-cell level. Such a spatio-temporal sharpening of neuronal signals at early central processing stages by inhibitory components is typical and widely present in other sensory systems such as the auditory (Adolphs, 1993; Suga, 1995), visual (Burkhardt and Fahey, 1998; Schiller, 1992) and somatosensory (Sachdev and Catania, 2002; Stanford and Hartline, 1980) system as well as in sensory specialists such as weakly electric fish. In the latter fish, processing of electrosensory inputs occurs in the hindbrain electrosensory lateral line lobe (ELLL) and also involves a reduction of receptive field size and contrast enhancement through a dedicated inhibitory microcircuitry. However, while such confinement of receptive fields in the ELLL is reminiscent of LTTD functionality in the IR system, the neuronal computations in weakly electric fish depend on descending inputs from the midbrain (Bastian, 1986), whereas the dynamic shaping of IR signals in the rattlesnake LTTD probably relies on local hindbrain circuitries.

Based on our results, the similarity between IR and other sensory systems with respect to central signal processing steps includes encoding and differentiation of motion direction. Such a feature has already been described for the auditory (Kuo and Wu, 2012; Wagner et al., 1994; Wagner and Takahashi, 1992), somatosensory (Lichtenstein et al., 1990; Wilent and Contreras, 2005) and visual system (Ariel and Daw, 1982; Barlow et al., 1964; Barlow and Hill, 1963). The magnitude of retinal ganglion cell discharge that encodes object motion depends strongly on the motion direction of the stimulus (Barlow et al., 1964; Barlow and Hill, 1963). In particular, individual retinal ganglion cells increase the discharge in response to a visual motion stimulus in the 'preferred' direction, and decrease the activity in the 'null' direction (Ariel and Daw, 1982; Barlow et al., 1964; Barlow and Hill, 1963). The mechanism underlying this directional selectivity in the retina derives from an asymmetric inhibition within adjacent sensory compartments (Barlow and Levick, 1965; Briggman et al., 2011). Such a computation also occurs in the synaptic processing of peripherally adjacent afferent inputs in LTTD neurons (Fig. 5D). The spatial asymmetry of excitatory and inhibitory response components in the latter neurons is generated by the different magnitudes of individual components from trigeminal nerve branches that innervate adjacent receptive areas of the pit membrane. Such a spatial asymmetry of inhibitory response components combined with a strong temporal contrast enhancement due to a delayed inhibition might ultimately assign directionally tuned edge-detection functionality to local LTTD microcircuits. Future experiments that employ more complex stimuli such as simulations of IR motion by transient electrical activation of afferents from adjacent receptive areas will clarify whether the computation within the LTTD also contributes to the detection of IR motion.

Acknowledgements

The authors also thank Yvonne Schwarz, Gabriele Schwabedissen and Michael Forsthofer for assistance with animal care and Dr Uwe Firzlaff for helpful comments on the manuscript.

Competing interests

The authors declare no competing or financial interests.

Author contributions

Conceptualization: M.S.B., H.L., H.S., T.K.; Methodology: H.S., T.K.; Software: M.S.B.; Validation: M.S.B., H.S., T.K.; Formal analysis: M.S.B., H.S., T.K.; Investigation: M.S.B.; Resources: H.L., H.S., T.K.; Data curation: M.S.B., H.L., H.S., T.K.; Writing - original draft: M.S.B., H.L., H.S., T.K.; Writing - review & editing: M.S.B., H.L., H.S., T.K.; Visualization: M.S.B.; Supervision: H.L., H.S., T.K.; Project administration: T.K.; Funding acquisition: T.K.

Funding

The authors acknowledge financial support from the German Science Foundation (Deutsche Forschungsgemeinschaft KO4835/1-1) and the German Federal Ministry of Education and Research (Bundesministerium für Bildung und Forschung) under Grant code 01 EO 0901.

References

Adolphs, R. (1993). Bilateral inhibition generates neuronal responses tuned to interaural level differences in the auditory brainstem of the barn owl. *J. Neurosci.* **13**, 3647-3668.

Amemiya, F., Ushiki, T., Goris, R. C., Atobe, Y. and Kusunoki, T. (1996). Ultrastructure of the crotaline snake infrared pit receptors: SEM confirmation of TEM findings. *Anat. Rec.* **246**, 135-146.

Ariel, M. and Daw, N. W. (1982). Pharmacological analysis of directionally sensitive rabbit retinal ganglion cells. *J. Physiol.* **324**, 161-185.

Baird, S. F. and Girard, C. (1853). *Catalogue of North American Reptiles in the Museum of the Smithsonian Institution. Part 1. Serpents*. Washington, DC: Smithsonian Institution.

Bakken, G. S. and Krochmal, A. R. (2007). The imaging properties and sensitivity of the facial pits of pitvipers as determined by optical and heat-transfer analysis. *J. Exp. Biol.* **210**, 2801-2810.

Barlow, H. B. and Hill, R. M. (1963). Selective sensitivity to direction of movement in ganglion cells of the rabbit retina. *Science* **139**, 412-412.

Barlow, H. B. and Levick, W. R. (1965). The mechanism of directionally selective units in rabbit's retina. *J. Physiol.* **178**, 477-504.

Barlow, H. B., Hill, R. M. and Levick, W. R. (1964). Retinal ganglion cells responding selectively to direction and speed of image motion in the rabbit. *J. Physiol.* **173**, 377-407.

Bastian, J. (1986). Gain control in the electrosensory system mediated by descending inputs to the electrosensory lateral line lobe. *J. Neurosci.* **6**, 553-562.

Biesdorf, S., Malinvaud, D., Reichenberger, I., Pfanzelt, S. and Straka, H. (2008). Differential inhibitory control of semicircular canal nerve afferent-evoked

inputs in second-order vestibular neurons by glycinergic and GABAergic circuits. *J. Neurophysiol.* **99**, 1758-1769.
Briggman, K. L., Helmstaedter, M. and Denk, W. (2011). Wiring specificity in the direction-selectivity circuit of the retina. *Nature* **471**, 183-188.
Bullock, T. H. and Diecke, F. P. J. (1956). Properties of an infra-red receptor. *J. Physiol.* **134**, 47-87.
Bullock, T. H. and Fox, W. (1957). The anatomy of the infra-red sense organ in the facial pit of pit vipers. *J. Microsc. Sci.* **98**, 219-234.
Burkhardt, D. A. and Fahey, P. K. (1998). Contrast enhancement and distributed encoding by bipolar cells in the retina. *J. Neurophysiol.* **80**, 1070-1081.
Chagnaud, B. P., Engelmann, J., Fritzsch, B., Glover, J. C. and Straka, H. (2017). Sensing external and self-motion with hair cells: a comparison of the lateral line and vestibular systems from a developmental and evolutionary perspective. *Brain Behav. Evol.* **90**, 98-116.
Chen, Q., Deng, H., Brauth, S. E., Ding, L. and Tang, Y. (2012). Reduced performance of prey targeting in pit vipers with contralaterally occluded infrared and visual senses. *PLoS ONE* **7**, 1-8.
Cook, P. B. and McReynolds, J. S. (1998). Lateral inhibition in the inner retina is important for spatial tuning of ganglion cells. *Nat. Neurosci.* **1**, 714-719.
de Cock Buning, T., Terashima, S.-I. and Goris, R. C. (1981). Crotaline pit organs analyzed as warm receptors. *Cell. Mol. Neurobiol.* **1**, 69-85.
Desalvo, J. A. and Hartline, P. H. (1978). Spatial properties of primary infrared sensory neurons in Crotalidae. *Brain Res.* **142**, 338-342.
Dräger, U. and Hubel, D. H. (1976). Topography of visual and somatosensory projections to mouse superior colliculus. *J. Neurophysiol.* **39**, 91-101.
Enroth-Cugell, C. and Lennie, P. (1975). The control of retinal ganglion cell discharge by receptive field surrounds. *J. Physiol.* **257**, 551-578.
Gilland, E. and Baker, R. (2005). Evolutionary patterns of cranial nerve efferent nuclei in vertebrates. *Brain Behav. Evol.* **66**, 234-254.
Goris, R. C. and Nomoto, M. (1967). Infrared reception in oriental crotaline snakes. *Comp. Biochem. Physiol.* **23**, 879-892.
Goris, R. C., Kadota, T. and Kishida, R. (1989). Innervation of snake pit organ membranes mapped by receptor terminal succinate dehydrogenase activity. *Curr. Herpetol. East Asia* 8-16.
Gracheva, E. O., Ingolia, N. T., Kelly, Y. M., Cordero-Morales, J. F., Hollopeter, G., Chesler, A. T. and Julius, D. (2010). Molecular basis of infrared detection by snakes. *Nature* **464**, 1006-1011.
Haverly, J. E. and Kardong, K. V. (1996). Sensory deprivation effects on the predatory behavior of the rattlesnake, Crotalus viridis. *Copeia* **1996**, 419-428.
Heric, T. M. and Kruger, L. (1965). Organization of the visual projection upon the optic tectum of a reptile (*Alligator mississippiensis*). *J. Comp. Neurol.* **124**, 101-111.
Kardong, K. V. and MacKessy, S. P. (1991). The strike behaviour of a congenitally blind rattlesnake. *J. Herpetol.* **25**, 208-211.
Kishida, R., Terashima, S.-I., Goris, R. C. and Toyokazu, K. (1982). Infrared sensory neurons in the trigeminal ganglia of crotaline snakes : Transganglionic HRP transport. *Brain Res.* **241**, 3-10.
Kohl, T., Bothe, M. S., Luksch, H., Straka, H. and Westhoff, G. (2014). Organotopic organization of the primary infrared sensitive nucleus (LTTD) in the western diamondback rattlesnake (*Crotalus atrox*). *J. Comp. Neurol.* **522**, 3943-3959.
Kuffler, S. W. (1953). Discharge patterns and functional organization of mammalian retina. *J. Neurophysiol.* **16**, 37-68.
Kuo, R. I. and Wu, G. K. (2012). The generation of direction selectivity in the auditory system. *Neuron* **73**, 1016-1027.
Lichtenstein, S. H., Carvell, G. E. and Simons, D. J. (1990). Responses of rat trigeminal ganglion neurons to movements of vibrissae in different directions. *Somatosens. Mot. Res.* **7**, 47-65.
Lynn, W. G. (1931). The structure and function of the facial pit of the pit vipers. *Am. J. Anatomy* **49**, 97-139.
Meszler, R. M., Auker, C. R. and Carpenter, D. O. (1981). Fine structure and organization of the infrared receptor relay, the lateral descending nucleus of the trigeminal nerve in pit vipers. *J. Comp. Neurol.* **196**, 571-584.
Moiseenkova, V., Bell, B., Motamedi, M., Wozniak, E. and Christensen, B. (2003). Wide-band spectral tuning of heat receptors in the pit organ of the copperhead snake (Crotalinae). *Am. J. Physiol. Regul. Integr. Comp. Physiol.* **284**, R598-R606.
Newman, E. A., Gruberg, E. R. and Hartline, P. H. (1980). The infrared trigemino-tectal pathway in the rattlesnake and in the python. *J. Comp. Neurol.* **191**, 465-477.
Noble, G. K. and Schmidt, A. (1937). The structure and function of the facial and labial pits of snakes. *Proc. Am. Philos. Soc.* **77**, 263-288.
Nowak, L., Bregestovski, P., Ascher, P., Herbet, A. and Prochiantz, A. (1984). Magnesium gates glutamate-activated channels in mouse central neurones. *Nature* **307**, 462-465.
Otto, J. (1972). Das Grubenorgan, ein biologisches System zur Abbildung von Infrarotstrahlern. *Biol. Cybern.* **10**, 103-106.
Rodieck, R. W. (1965). Quantitative analysis of cat retinal ganglion cell response to visual stimuli. *Vision Res.* **5**, 583-601.
Roelke, C. E. and Childress, M. J. (2007). Defensive and infrared reception responses of true vipers, pitvipers, azemiops and colubrids. *J. Zool.* **273**, 421-425.
Sachdev, R. N. S. and Catania, K. C. (2002). Receptive fields and response properties of neurons in the star-nosed mole's somatosensory fovea. *J. Neurophysiol.* **87**, 2602-2611.
Schiller, P. H. (1992). The ON and OFF channels of the visual system. *Science* **15**, 86-92.
Schroeder, D. M. and Loop, M. S. (1976). Trigeminal projections in snakes possessing infrared sensitivity. *J. Comp. Neurol.* **169**, 1-13.
Stanford, L. R. and Hartline, P. H. (1980). Spatial sharpening by second-order trigeminal neurons in crotaline infrared system. *Brain Res.* **185**, 115-123.
Stanford, L. R. and Hartline, P. H. (1984). Spatial and temporal integration in primary trigeminal nucleus of rattlesnake infrared system. *J. Neurophysiol.* **51**, 1077-1090.
Straka, H., Biesdorf, S. and Dieringer, N. (1997). Canal-specific excitation and inhibition of frog second-order vestibular neurons. *J. Neurophysiol.* **78**, 1363-1372.
Suga, N. (1995). Sharpening of frequency tuning by inhibition in the central auditory system: tribute to Yasuji Katsuki. *Neurosci. Res.* **21**, 287-299.
Terashima, S.-I. and Goris, R. C. (1977). Infrared bulbar units in crotaline snakes. *Proc. Jpn Acad. Ser. B Phys. Biol. Sci.* **53**, 292-296.
Terashima, S.-I. and Liang, Y. F. (1991). Temperature neurons in the crotaline trigeminal ganglia. *J. Neurophysiol.* **66**, 623-634.
Terashima, S.-I., Goris, R. C. and Katsuki, Y. (1968). Generator potential of crotaline snake infrared receptor. *J. Neurophysiol.* **31**, 682-688.
Terashima, S.-I., Goris, R. C. and Katsuki, Y. (1970). Structure of warm fiber terminals in the pit membrane of vipers. *J. Ultrastruct. Res.* **31**, 494-506.
van Dyke, J. U. and Grace, M. S. (2010). The role of thermal contrast in infrared-based defensive targeting by the copperhead, Agkistrodon contortrix. *Anim. Behav.* **79**, 993-999.
Wagner, H. and Takahashi, T. (1992). Influence of temporal cues on acoustic motion-direction sensitivity of auditory neurons in the owl. *J. Neurophysiol.* **68**, 2063-2076.
Wagner, H., Trinath, T. and Kautz, D. (1994). Influence of stimulus level on acoustic motion-detection sensitivity in barn owl midbrain neurons. *J. Neurophysiol.* **71**, 1907-1916.
Westhoff, G. (2014). Giftschlangen und Krustenechsen. In *Sachkunde Gefährliche Reptilien* (ed. A. S. Henning), pp. 32-42. Mannheim, Germany: VDA/DGHT Sachkunde GbR.
Westhoff, G., Morsch, M. and Ebert, J. (2006). Infrared detection in the rattlesnake *Crotalus atrox*–from behavioural studies to midbrain recordings. In Proceedings of the 13th Congress of the Societas Europaea Herpetologica, pp. 225-228.
Wilent, W. B. and Contreras, D. (2005). Dynamics of excitation and inhibition underlying stimulus selectivity in rat somatosensory cortex. *Nat. Neurosci.* **8**, 1364-1370.